ADVANCED GROUND-PENETRATING, IMAGING RADAR

FOR BRIDGE INSPECTION

John P. Warhus, Jeffery E. Mast, Erik M. Johansson, Scott E. Nelson
University of California
Lawrence Livermore National Laboratory
Electronics Engineering Department
P.O. Box 808
Livermore, CA 94550

Hua Lee
University of California
Santa Barbara
Electrical and Computer Engineering
Santa Barbara, CA 93106-9560

INTRODUCTION

Inspecting high-value structures, like bridges and buildings using Gound Penetrating Radar (GPR) is an application of the technology that is growing in importance. In a typical inspection application, inspectors use GPR to locate structural components, like reinforcing bars embedded in concrete, to avoid weakening the structure while collecting core samples for detailed inspection. Advanced GPR, integrated with imaging technologies for use as an NDE tool, can provide the capability to locate and characterize construction flaws and wear- or age-induced damage in these structures without the need for destructive techniques like coring.

In the following sections, we discuss an important inspection application, namely, concrete bridge deck inspection. We describe an advanced bridge deck inspection system concept and provide an overview of a program aimed at developing such a system. Examples of modeling, image reconstruction, and experimental results are presented.

BACKGROUND

An advanced GPR-based inspection system has the near-term potential of addressing critical national and international needs for reliable, cost effective NDE of bridges and other reinforced concrete structures. There are more than 578,000 highway bridges in the US and more than 40 percent of them are either structurally deficient or functionally obsolete [1]. These conditions limit bridge utility and, if they are not properly monitored and maintained, can pose a safety threat to the bridge users.

The bridge deck and its wearing surface are the most vulnerable parts of a bridge to damage from routine service, and they are particularly well suited for inspection using a vehicle mounted inspection system. The deck has a shorter average service life (35 years) than the bridge itself (68 years). The wearing surface, which provides the driving surface and protects the deck beneath it, is usually designed to be replaced many times over the life of the bridge. Concrete slabs with concrete or asphalt wearing surfaces are the most widely used decks in all types of bridge constructions [2].

In recent research applications, GPR was evaluated to determine its ability to accurately and rapidly characterize the condition of roadbeds and bridge decks [3, 4]. Those studies showed that GPR, when integrated with appropriate computers and software, can improve the efficiency and accuracy of inspection of roadbeds and bridge decks. However, the measurement techniques used in each case produced data of limited usefulness for detailed condition assessments. For example, in both cases GPR data were collected only in the vehicle wheel paths. These measurements were used to extrapolate the overall deck or roadbed condition-estimate based on layer reflectivity. Because of the limited data acquisition, the techniques used in these studies could not provide information needed to map damaged areas. That information is required if economical repairs, short of major restoration or replacement, are to be implemented. In addition, in both studies, only the down-range (depth) resolving capabilities of GPR were used to assess roadbed or deck conditions; significant additional data can be obtained from GPR surveys if cross-range (transverse) resolving capabilities are also used.

In an advanced bridge deck inspection system, like the one described below and in [5 and 6], a mobile GPR gathers data for later high-resolution image reconstruction of embedded defects and features. High-quality images allow visualization of structure internals, permitting evaluation of condition with data that usually is obtainable only with destructive methods. Performance enhancements are achieved by the application of advanced hardware and software. Traffic-lane-wide coverage is enabled by the use of new transmitters, antennas, and large-aperture receiving arrays. High-speed data acquisition and accompanying inspection vehicle speed are feasible with multiple receiver channels using state-of-the-art data transmission and storage equipment. Overall resolution is improved by increased transmitter pulse bandwidth and enhanced antenna performance. Cross-ranging capabilities are exploited by applying synthetic aperture radar data processing techniques to produce three-dimensional spatial images.

ADVANCED GROUND-PENETRATING IMAGING RADAR (GPIR) CONCEPT

The system concept for an advanced GPIR system is illustrated in Figure 1. An inspection vehicle equipped with a transmitting antenna and a linear array of receivers travels over the bridge deck, sweeping out a traffic-lane-wide synthetic aperture. Data recorded from the receivers is transferred via multiple data streams to a mass data storage subsystem, from which it can be accessed for image reconstruction. Transmitter power and receiver sensitivity levels permit data acquisition to depths of 0.5 m in the deck. High-speed image processing computers, in centrally-located processing centers, reconstruct images of the bridge deck structure for evaluation by a bridge inspector. High-resolution three-dimensional images for a typical bridge are reconstructed in less than one hour. Images have resolution limits of ~12.5 mm in depth and 50 to 100 mm in azimuth.

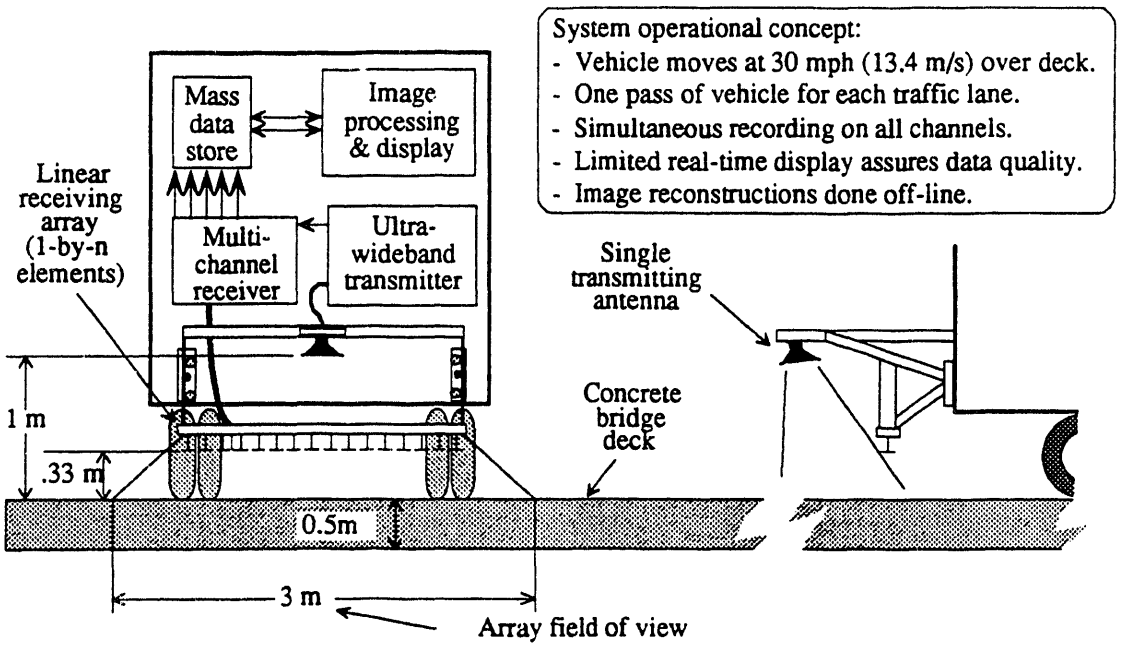

Figure 1. Advanced GPIR bridge deck inspection system concept.

CONCEPT DEVELOPMENT

Our approach to development of system and subsystem concepts for an advanced bridge inspection system has involved modeling, experiments, design and test of advanced GPR components, and development of unique image reconstruction techniques. These elements were combined to permit theoretical and experimental evaluation of the feasibility of the overall concept. The following sections provide a brief overview of our modeling, experimental and imaging development efforts.

Material characterization, modeling and image reconstruction

To better understand the problem of collecting radar data from and producing images of features embedded in a lossy heterogeneous material like concrete, we performed broadband (0.1 to 4 GHz) scattering parameter measurements (transmission and reflectivity) of cement samples. These measurements were made using a network analyzer and a coaxial air-line in which a portland cement sample replaced the air dielectric surrounding the center conductor. From measured parameters we calculated the frequency-dependent permittivity and characterized attenuation for cement. Measurements were made over a period of months to observe changes in these properties as the cement cured.

We used the results of the cement characterization measurements and analyses, combined with known properties of aggregate materials, to define the dominant electrical properties of concrete needed to accurately model the material. To validate the model, a one-dimensional (1-D) simulation of the scattering parameter measurement setup was implemented using the finite-difference time-domain (FDTD) electromagnetic (EM) simulation code AMOS. Figure 2 shows the measurement setup and measured and simulated results. Good agreement between measurement and simulation provided validation of the cement model.

We extended these 1-D results to two-dimensions both experimentally and in simulation. In an experiment, we launched ultra-wide-band (UWB) pulses through a concrete block, and detected and recorded the EM energy transmitted through the block. A

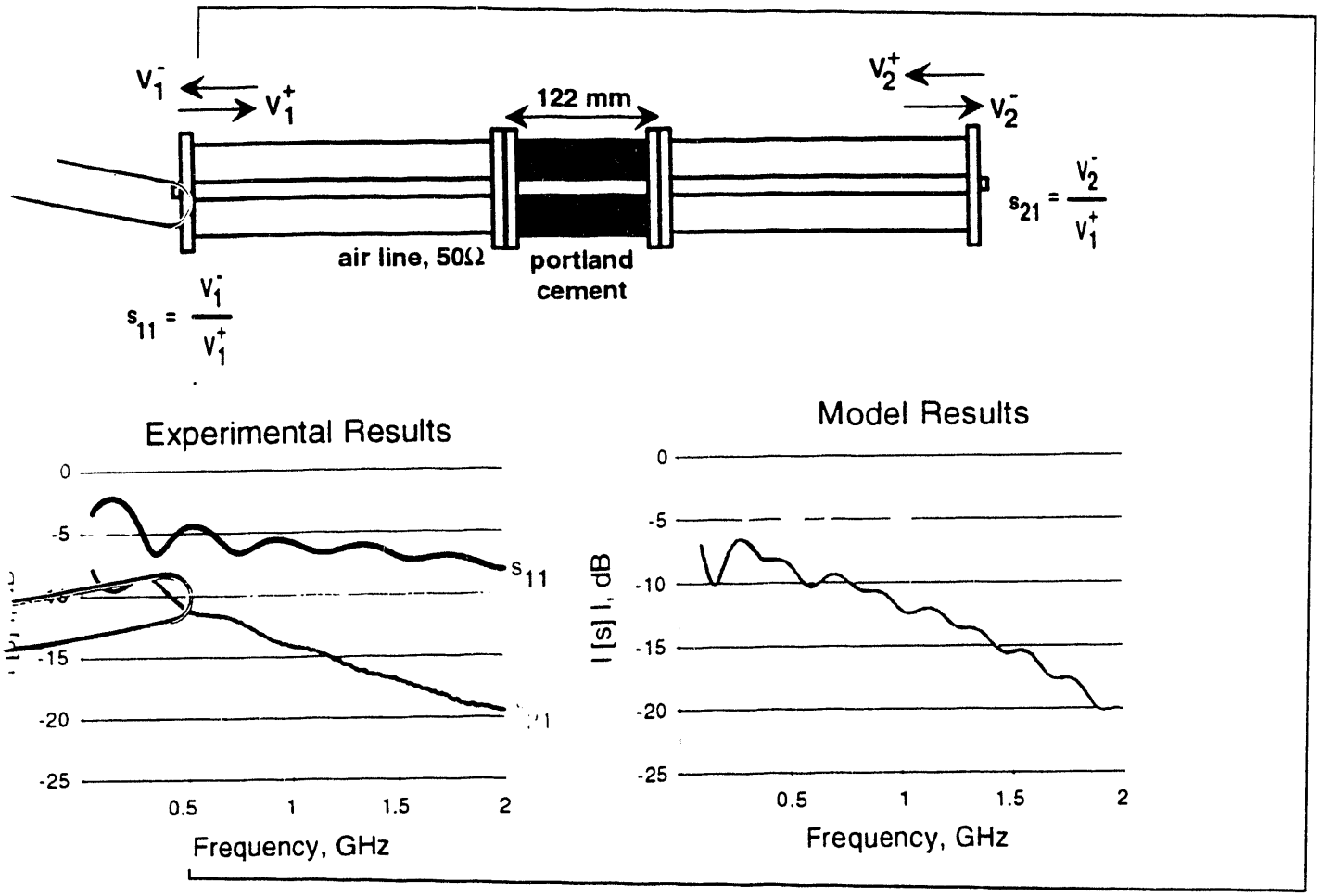

Figure 2. Material characterization: Scattering parameter measurements and simulation

two-dimensional (2-D) model of the experiment was constructed and run using AMOS. The model used the complex permittivity model from the 1-D case, and included such details as antenna beamwidth, radiated electric field waveform, dimensions of the block, dispersive and clutter effects produced by the cement and the aggregate within it. Fig. 3 shows the experimental setup and plots of both the experimental measurements and simulated results. Again, there is good agreement between experiment and simulation.

After confirming the validity of our 2-D EM model for concrete, this analytical tool was used extensively to evaluate radar system design parameters. Parametric studies we conducted using this model are summarized in Table 1. Image reconstructions were made from the simulated radar data for most of the cases listed in the table. The images aided assessments of the impacts of design parameter changes on overall system performance and complexity, and in evaluating image quality for specific imaging techniques. In addition to the studies listed in the table, 2-D simulations permitting evaluation of air/concrete boundary and antenna cross-coupling effects, and impact of using multiple transmitters, as well as multiple receivers were also run. These studies helped to confirm conceptual design conclusions and permitted consideration of more complex system configurations.

Figure 4 shows an example of a typical modeling problem. In this 2-D case, a transmitting antenna illuminates a layered media consisting of air, asphalt and concrete layers. Four rebar-like targets are embedded in the concrete layer which also contains aggregate. A linear array of reveiving antennas located in air close to the air-asphalt interface senses EM energy directly from the transmitter and scattered from the layer boundary interfaces, and targets and clutter within each layer. Time slices from the

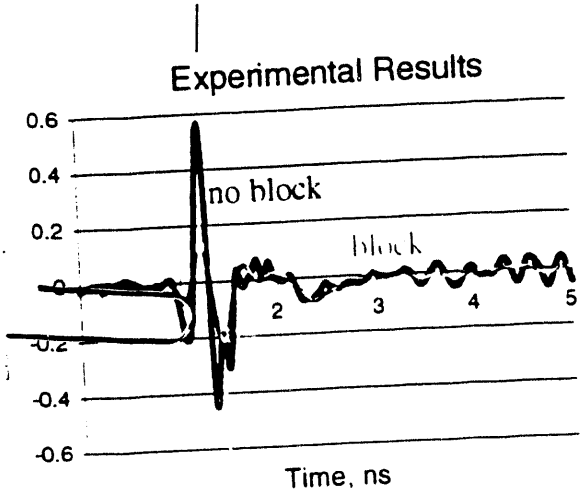

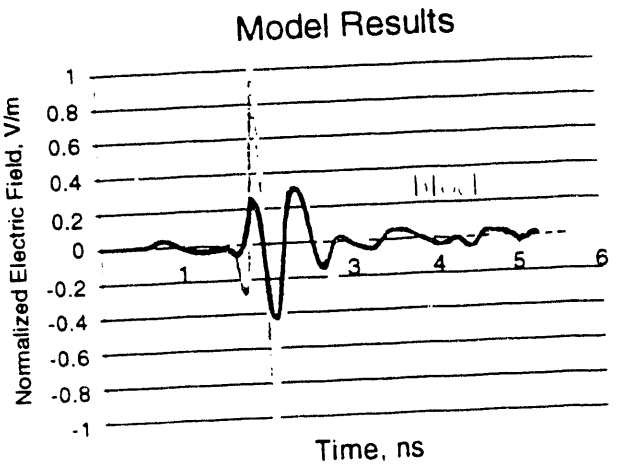

Figure 3. Model validation in two-dimensions

Table 1. Model-based parametric studies

Parameter	Variations
Radiated Pulsewidth	100 to 1000 picoseconds
Spatial Sample Rate	5 to 45 millimeters
Target Cross-section	5 to 75 millimeters
Target Depth	10 to 150 millimeters
Clutter Source (aggregate) Density	10 to 50 percent
Cross Range Resolution	Target spacing:
Layered media	Layer thickness: 25 to 210 mm Layer composition: air, asphalt, concrete (variable aggregate density and dielectric constants for concrete and asphalt layers)
Target Density/Type	No targets, 1 void, 2 reinforcing bars (re-bars), 2 re-bars + 1 void, a re-bar grate, and re-bar shaded from EM radiation by other re-bars

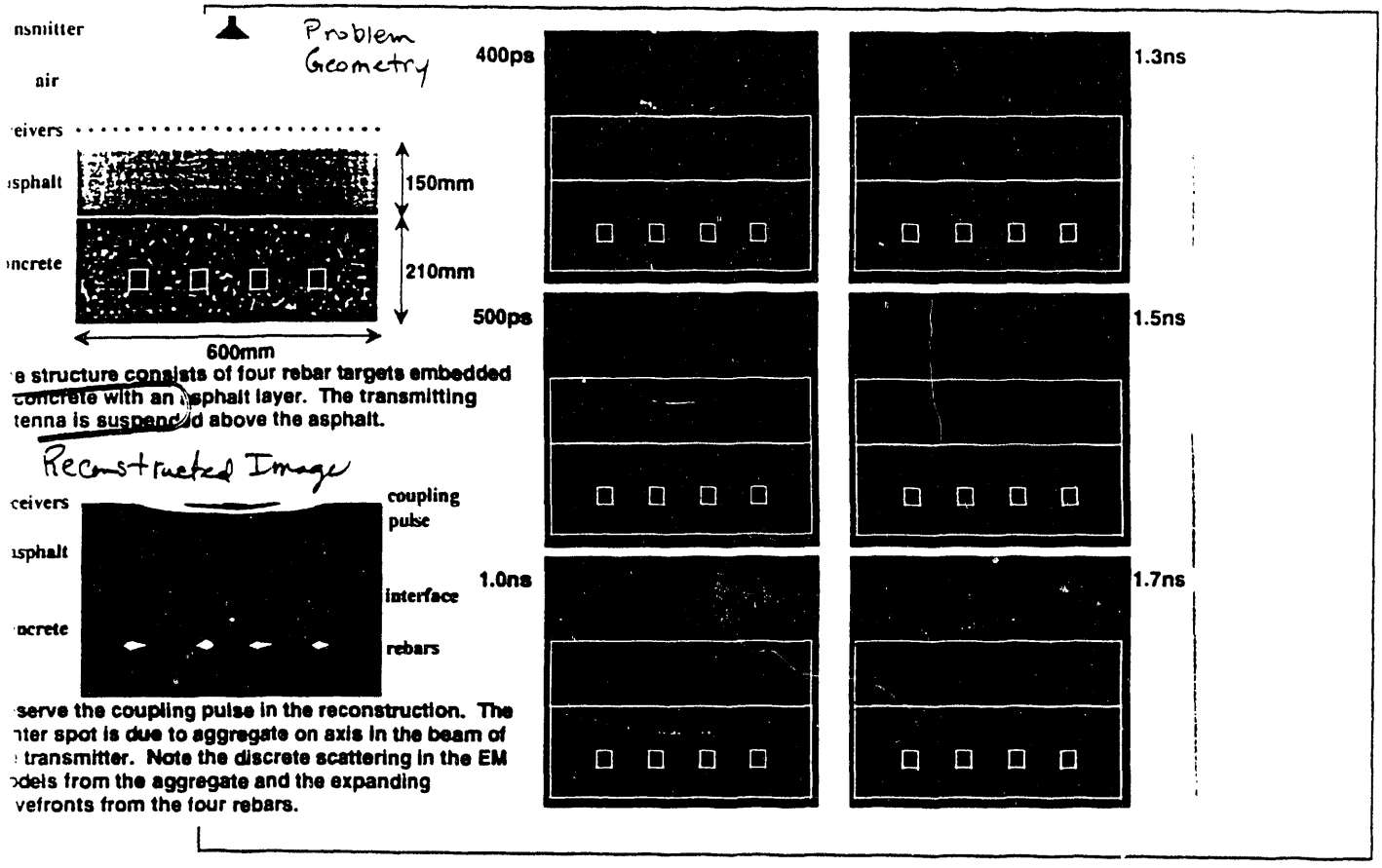

Figure 4. A typical 2-D modeling and image reconstruction example

simulation are shown in sequence to illustrate the interactions that occur as the EM energy propagates through the problem space. The reconstructed image clearly shows the rebar targets, layer boundaries, and clutter.

Recent Experimental Results

In recent testing, we collected data and reconstructed images of features embedded within a concrete test bed. In these experiments, we collected data using a monostatic antenna configuration driven by a low-power impulse generator (~ 1 watt, peak). The antennas were mounted on a motor-driven slider 50 mm above the concrete surface, and moved over of the test bed while data were collected over a square sampling grid at 1.7 mm spatial intervals.

Our test bed (Figure 5) is a concrete slab containing reinforcing bars, both fixed and removable, and other objects designed to provide a means for evaluating data acquisition and imaging performance. Concrete poured in the test bed was prepared in accordance with specifications used by the California Department of Transportation for concrete bridge decks. The test bed is equipped with motor-driven slide mechanisms which permit antennas to be accurately and repeatably moved over the slab, simulating both the movement of an inspection vehicle over a bridge deck and the linear array of receiving antennas mounted on the vehicle. Figure 6 shows a sequence of 2-dimensional images which are planar slices from a 3-dimensional image reconstruction; the slices are parallel to the concrete surface. The depth calculated in the reconstruction is indicated for each frame. The sequence starts near the surface (Frame A) and progresses through the volume. Within the imaged volume are four cylindrical voids; these voids are in locations where removable reinforcing bars(rebars) have been removed. The first two voids are

Figure 5. The GPR laboratory showing a typical experimental setup

parallel with each other and nearly parallel with the concrete surface. One of the voids, at the top of the image, is only partially visible in Frames C through E; the other is visible in Frames B through E. The third void is beneath and perpendicular to the first two, and it slopes slightly deeper into the concrete at the end near the top of the image. The third void first appears near the bottom of Frame D and is visible through Frame G. The difference in depth, within the image, from one end of the third void to the other is approximately 18 mm; its sloping orientation is evident in the image sequence. Part of the fourth void is visible in the lower right corner of Frames G and H of the sequence. This void starts at a depth of about 100 mm and slopes deeper into the concrete and toward the top of the frame. The low output power of the impulse generator used in this experiment, limited our ability to detect objects deeper than about 115 mm in the concrete.

Figure 7 shows a similar sequence of 2-dimensional planar slices from another experiment. Data were collected over the same area of the test bed, but the size and shape of the area were altered slightly to include a more complete view of features near the concrete surface. For this experiment, rebars were installed in three of the cylindrical voids shown in the previous example. In one of the voids nearest the surface, rebars were installed to form a 100 mm long cylindrical air gap in the imaged volume. The first two parallel rebars begin to appear in Frame B and are visible through Frame E. The rebar near the top of the image has the air gap clearly visible in Frames C through E. Although the parallel rebars are the same size (25 mm diameter), their images do not have the same intensity. This difference is a result of the rebars having different scattering cross sections; instead of being round, the rebars have a somewhat irregular oval shape making their cross sections orientation-dependent. Rebars used to form the 100 mm void were oriented to provide a larger cross section (and thus a relatively larger scattered signal), while the rebar in the other void was oriented to provide a smaller cross section. The third rebar is perpendicular to and beneath the first two and is visible in Frames D through G.

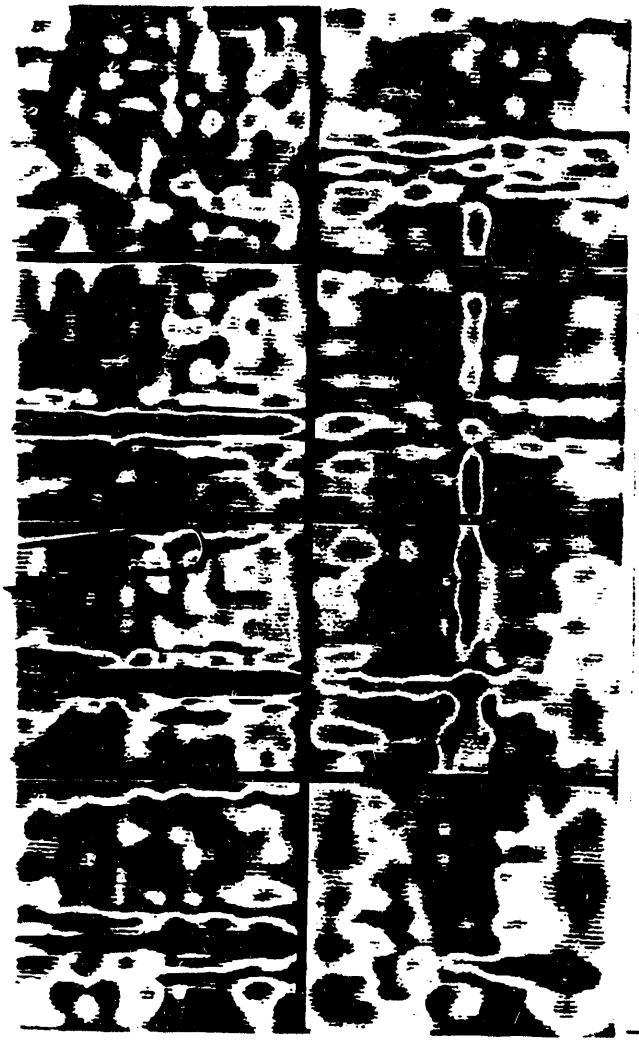

Figure 6. Image sequence: 4 cylindrical voids embedded in concrete.

CONCLUSIONS

GPR combined with unique image reconstruction algorithms developed for identification and characterization of subsurface flaws and structural features has the potential for providing rapid and cost-effective methods for large-area inspection of bridge decks. A basic inspection system design concept was described which is being developedat LLNL and used to guide development of GPR hardware and imaging algorithms. A laboratory testing capability, supported with both standard and specially developed equipment and extensive computational modeling capability, has been established to evaluate GPR components, subsystems, and systems. Recent test and image processing results have produced high quality reconstructed images of subsurface test objects. The results show that the basic inspection concept is feasible.

ACKNOWLEDGEMENTS

Work performed under the auspices of the U.S. Department of Energy by Lawrence Livermore National Laboratory under Contract no. W-7405-Eng-48.

REFERENCES

1. "Our Nation's Highways: Selected Facts and Figures"; US Department of Transportation, Federal Highway Administration; Publ. No. FHWA-PL-90-024.

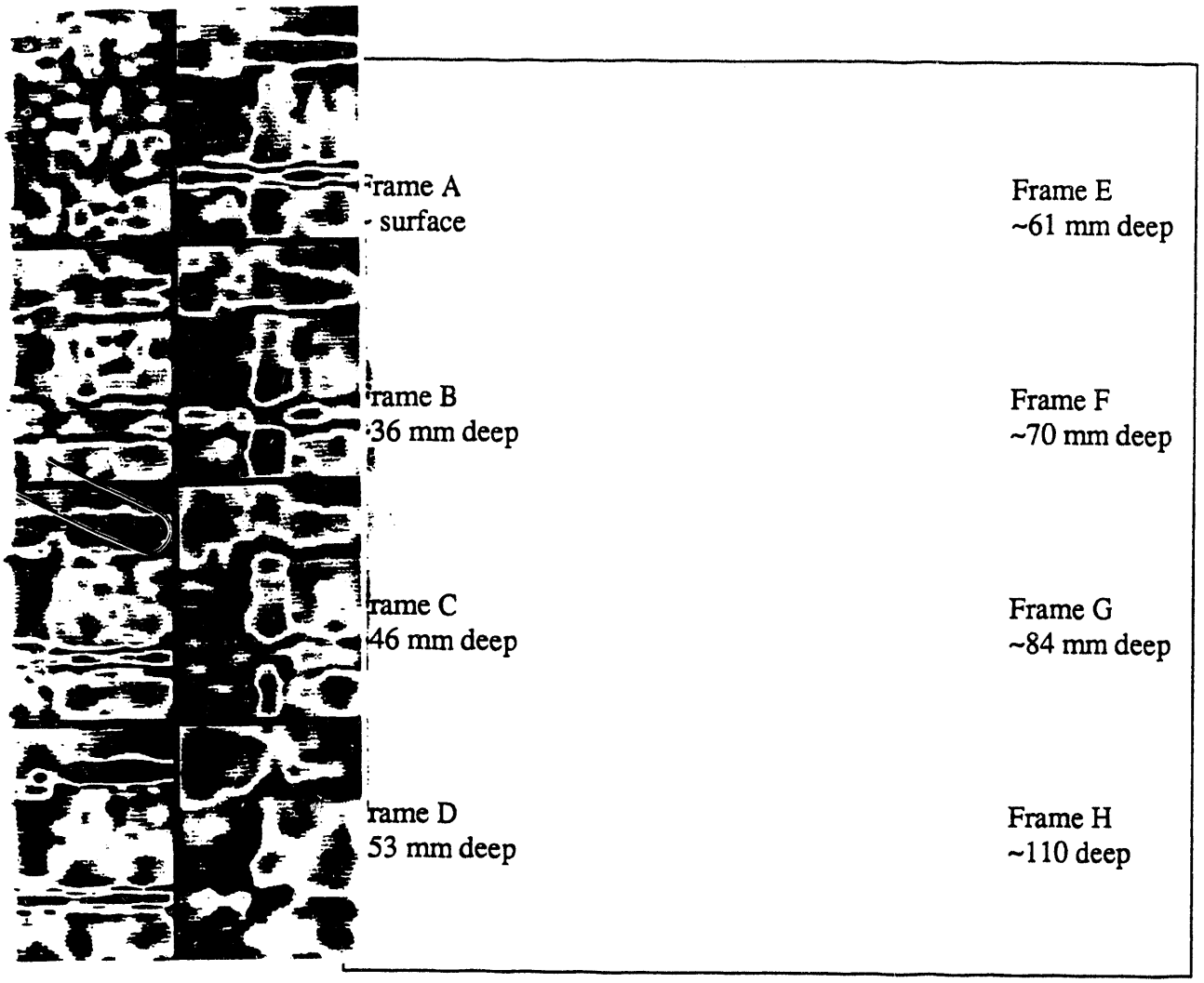

Figure 7. Image sequence: 3 rebars embedded in concrete.

2. Jones and B.R. Ellingwood, "NDE of Concrete Bridges: Opportunities and Research Needs," *Federal Highway Administration Conf. on NDE for Bridges*, Arlington, VA, (August 25-27, 1992).

3. Infrasense, Inc., *Final Report, Bridge Deck Evaluation Utilizing High Speed Radar*, prepared for the New Hampshire Department of Transportation Bureau of Materials and Research, Concord, NH (November 1991).

4. K.R. Maser, T. Scullion, and R.C. Briggs, *Use of Radar Technology for Pavement Layer Evaluation*, Texas Transportation Institute, College Station, prepared for Federal Highway Administration, Austin, TX (February 1991).

5. J.P. Warhus, J.M. Hernandez, S.D. Nelson, E.M. Johansson, and H. Lee, "Ground Penetrating, Imaging Radar for Bridge Inspection," *Engineering Research, Development, and Technology Thrust Area Report FY-92*, Lawrence Livermore National Laboratory, Livermore, CA UCRL 53868-92, (March 1993).

6. J.P. Warhus, J.E. Mast, S.D. Nelson, and E.M. Johansson, *Ground-Penetrating Imaging Radar Development for Bridge Inspection*, Lawrence Livermore National Laboratory, Livermore, CA UCRL-ID-113954 (May 1993)

END

DATE
FILMED
3/10/94